A Novel Diagnostic Technique for Open-Circuited Faults of Inverters Based on Output Line-to-Line Voltage Model

Cheng Shu, Chen Ya-Ting, Yu Tian-Jian, and Wu Xun

***Abstract*—An output line-to-line voltage model-based fault diagnostic technique is presented in this paper. From the theoretical analysis of the output voltage under normal and faulty conditions, a preprocessing method is developed to extract fault features from diagnosis eigenvalue. A voltage envelope line is generated by the proposed voltage envelope function. By comparing the preprocessed diagnosis eigenvalue and the voltage envelope, single-switch open-circuit faults can be located precisely. Because the proposed method does not rely on the accurate amplitude of the output line-to-line voltage, the influence of the load changing is minimized and simple hardware is adopted, which has advantages of low cost, high reliability, and short diagnosis time. Moreover, as long as the inverter output voltages have the feature of periodic nonpositive and nonnegative, this method is valid no matter what control strategy is adopted by the inverter and no control signal is required for the diagnosis process. The prototype system is tested to validate the adaptability of the proposed method under different conditions, such as the diverse loads, various control strategies, and fault-occurrence time.**

***Index Terms*—Fault diagnosis, fault location, inverters, open-circuit fault.**

I. Introduction

PWM technology-based inverters are widely used in industrial field. Its reliability is of crucial importance. However, the inverter faults are inevitable at the present stage. Consequently, fault-diagnosis technology of inverters is becoming a research hotspot recently. The industrial inverter system faults are mainly caused by capacitor failures, semiconductor switches' breakdowns, and driving circuit misfire [1]. The reported fault diagnosis methods can be divided into two categories by their different diagnosis objectives.

In the first category, the reported methods aim at the inverters' component faults. Capacitor faults are discussed in [1]–[4] and [24]. Insulated gate bipolar transistor (IGBT) failures are analyzed in [5] and [6]. A circuit model-based parameter identification method is presented in [1] to identify the equivalent series resistance (ESR) and deduce the trend of ESR. In [2], when the motor is stopped, the ESR and capacitance of the dc-link aluminum electrolytic capacitors are calculated by recursive least square method. Then, the ESR and capacitance are used for fault diagnosis and life prediction. In [3], by injecting a controlled ac current component into the input, ac voltage ripples on the dc output can be induced. The value of the ESR is then calculated by manipulating these ac voltages and current components with digital filters. The temperature effect is also considered in [3]. In [4], different influences of hysteresis current control and pulse width modulation (PWM) techniques on power factor correction (PFC) output filtering capacitors are discussed, and a new electric equivalent scheme of electrolytic capacitors is determined using genetic algorithms. Because ESR will increase at high frequencies due to skin effect, the frequency augment is taken into account in [4]. A low-cost bandpass analog filter centered at a high frequency is proposed in [5] to evaluate the converter parameter variations over time. The parameters' variations are characterized from ringing, and they are used to assess the aging status of transistor in the power electronic circuits and electric machines. The wire-bond-related failures are investigated using the ON-state voltage drop as a failure indicator in [6], the proposed method can achieve accurate online testing by injecting external currents into the power unit during the idle time. This category of fault diagnosis method requires a thorough understanding of the physical characteristic and structure of components. These methods are easily influenced by environmental change, and it is difficult to verify their performance. Moreover, their applications are limited by fault model accuracy and fault feature extraction difficulties.

Another category is formed with methods aiming at topology faults. There are two kinds of inverter topology faults that are switch open-circuit and switch short-circuit fault. The switch short-circuit fault has great damage to inverter. As a result, reliable protection circuits are added to protect components and shutdown inverter when switch short-circuit fault happens. The switch open-circuit fault is not as destructive as short-circuit fault, and switch open-circuit fault do not necessarily cause the inverter breakdown immediately. However, switch open-circuit fault may cause the secondary damage to other components and may crash the inverter eventually. The fault diagnosis methods of this category have been reported in [7]–[23]. Four detection techniques of voltage-fed asynchronous machine drive systems have been introduced and compared in [7]. An inverter output voltage-based method is proposed in [8] to diagnose

Manuscript received September 6, 2015; revised December 25, 2015 and January 25, 2016; accepted January 26, 2016. Date of publication February 29, 2016; date of current version June 9, 2016. This work was supported by the National Natural Science Foundation of China under Grant 61273158.

The authors are with the School of Traffic and Transportation Engineering, Central South University, Changsha 410075, China (e-mail: chengshu@csu.edu.cn; 151341119@qq.com; 250486154@qq.com; 309931624@qq.com).

Digital Object Identifier 10.1109/TIE.2016.2535960

the short-circuit fault in a time-free domain that is called the voltage space, the fault detection time is short and the fault detection and isolation (FDI) result does not depend on the load, the PWM frequency and the feedback loop. But this method cannot diagnose open-circuit fault. A novel diagnostic algorithm is proposed in [9]. The algorithm is quite simple, and it just requires the measured motor phase currents and their corresponding reference signals to diagnosis faults. This method can diagnose 27 kinds of open-circuit faults. In [10], an algorithm for multiple open-circuit faults diagnosis in full-scale back-to-back converters is presented; the phase current is processed to be independent to the operating conditions and then adopted as the diagnosis eigenvalue. But the computational quantity of [9] and [10] is relatively large, the diagnosis accuracy and speed are subject to the choices of empirically threshold. In [11], PWM switching signals and the output line-to-line voltages are analyzed during the switching time of voltage source inverter (VSI)-fed induction motor drives. This method achieves not only accurate single and multiple switches' fault diagnosis but also minimization of the fault detection time, which is one switching period maximum. Voltage difference of lower switches between faulty and normal states is used in [12] to detect the open-circuit fault. The difference of line voltages during the PWM_ON and PWM_OFF time is considered as the fault feature in [13]. Methods in [12] and [13] employ simple hardware circuits and achieve a very short diagnosis time. In [14], the slope of the inductor current is adopted as the diagnosis evidence and is observed over time, two parallels of working fault detection (FD) subsystems are also adopted as a hybrid structure to perform fast diagnosis. A voltage-based approach for open-circuit fault diagnosis in closed-loop controlled PWM converters is proposed in [15], and this method does not require any additional sensors. Although paper [11]–[15] each has its advantages, they need trigger signal or reference signal of controller as the diagnosis eigenvalue. Therefore, a modification on the original inverter control system is inevitable, and there is also the possibility of increasing potential fault risk. These drawbacks will greatly limit the application of these methods, especially in the inverters that are already in service. A switch open-circuit fault detection method and diagnosis system for matrix converters is presented in [16]. No-load models, averaging windows, or additional sensors are needed for this method. But adjustment to original converter and the acquisition of switch state are required. An FDI method is proposed in [17] for the EV. This method is based on the phase currents' instantaneous frequency and envelope. Specific operating conditions are also taken into account, such as the flux-weakening region and energy recovery. An improved normalized dc-components-based diagnosis method is proposed in [18]. A d–q voltage offset observer is designed to detect open-switch fault in [19]. A Concordia current pattern radius-based method is present in [20]. Complex calculation and detection delay are the drawbacks of [17]–[20].

Some of the above diagnosis methods require trigger signal as one of the diagnosis eigenvalues, and some of them need to incorporate the diagnosis hardware into the original inverter control system. Furthermore, there are methods employ additional sensors. All these implementations will possibly increase the potential fault points and lower the practicability. Some of other methods adopt the load current as the diagnosis eigenvalues, this kind of methods is relatively easier affected by load changing, and their fault diagnosis time is commonly longer than voltage-based methods. Also, there are reported methods having the disadvantages of large computational complexity and hardware cost. Each of the above drawbacks may cause a serious limitation in practical applications.

Because the switch short-circuit faults can be easily transferred into switch open-circuit faults by means of fast fuses [9], [25], [26], this paper is mainly focusing on switch open-circuit faults of inverter. The operation principle of passenger train onboard inverter has been researched under both normal and abnormal states. The proposed method does not require inverter control signals. Normally, the single switch open-circuit faults can be located in one carrier period. Moreover, the proposed method has excellent robustness, and its accuracy is independent from load variation. The proposed method can also be applied to sinusoidal pulse width modulation (SPWM), space vector pulse width modulation (SVPWM), and other control strategies-based inverters whose output line-to-line voltages have periodic nonpositive and nonnegative values. A simple and cheap hardware is employed to achieve low cost and high reliability. All the features above jointly make the proposed method not only suit for newly built inverters but also the inverters already in service. With few adjustments, the proposed method can be used in other inverters with fixed output voltage frequency.

Section II presents an overview of the objective system as well as the general idea of the proposed method. Section III puts forward a proposition, and analyzes the operation of the inverter with the proposition. Section IV proposed a fault diagnosis method, and take T_1 open-circuit fault as an example to illustrate how to apply the proposed method on the objective inverter. The affecting factors are discussed in Section V and the experimental results are analyzed in Section VI. Section VII concludes this paper.

II. System Overview

A. Operational Principle of Objective System

Type 25T passenger train adopts disperse conversion topology to supply power to onboard electric devices. There is a hot standby redundancy inverter for each passenger train. When the active inverter breakdown, loads are supplied by the hot standby redundancy inverter, so the onboard electric devices of type 25T passenger train are working uninterrupted. The input voltage of the inverter is dc 600 V, and the output voltage is three-phase 380 V/50 Hz. SPWM is adopted. The schematic diagram of the inverter is shown in Fig. 1.

In Fig. 1, T_1-T_6 are the IGBTs; normally, the IGBT body diode has greater forward voltage and junction–case thermal resistance than IGBT itself. Therefore, to ensure the systems' reliability during the freewheeling period, D_1-D_6 in Fig. 1 are additional reverse parallel diodes for IGBTs (not the body diodes of T_1-T_6); dc-side support capacitor is composed of $C_{11}-C_{14}$ and $R_{11}-R_{14}$, which are used to stabilize the dc input voltage for inverter; contactor KM2 and resistor R_{10} are

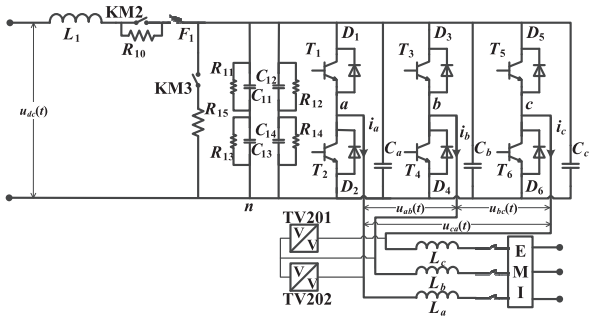

Fig. 1. Diagram of the inverter on Type 25T passenger train.

working together as a precharge circuit to limit input current during the start-up process; the discharge circuit, which is composed of KM3 and R_{15}, releases electricity stored in support capacitor after inverter stops; L_1 is the input reactor; $L_a - L_c$ are the output filtering inductors; and $C_a - C_c$ are the inductance-free capacitors.

B. General idea of the New Diagnosis Method

From the perspective of statistical data in recent research, almost 70% of converter faults are more or less related to power switches, such as open- or short-circuit fault, gate misfiring, and so on [24]. Most inverters are protected from overcurrent by fast fuses. Once switches encounter short-circuit faults, the fast fuses cutoff the faulty switches instantly. For the inverters without protection, it is also convenient to add fast fuses. Therefore, short-circuit fault will be transformed into open-circuit fault in most cases. Meanwhile, the phenomenon of gate-misfiring faults is similar to that of switch open-circuit faults. Thus, this paper focuses on the research of switch open-circuit faults.

The most direct characteristic information is contained in three-phase output voltages when switch open-circuit fault occurs. Furthermore, the output voltages are independent to load changes. Therefore, three-phase output voltages collected by TV201/202 in Fig. 1 are selected as diagnosis eigenvalues. An output line-to-line voltage envelope function is proposed based on the fixed periodicity trait of inverters' output. Output line-to-line voltages are preprocessed and combined with the envelope line to extract fault characteristics caused by switch open-circuit fault. Then, the faulty switch is located.

The proposed fault diagnosis method employs a low-cost simple hardware. The diagnosis process can be completed in one carrier period. The whole diagnosis process is irrelevant to load change. Moreover, no control signal is needed, so the proposed method is independent to both dead zone and ON–OFF delay of switch.

III. Analysis of Inverter Operation

A. Normal Operation of Inverter

SPWM is adopted by the passenger trains' onboard inverter. The basic operating principle of SPWM is that, the control trigger pulses are generated by comparing a carrier signal $c_t(t)$ to a reference signal $r_\varphi(t)$. The definition of reference signal $r_\varphi(t)$ is shown in (1), where u_r, T_r, and f_r are the amplitude, period, and frequency of the reference signal, respectively. θ_φ is the displacement angle which has the values 0, $-2\pi/3$, and $2\pi/3$ for $\varphi = A, B, C$ three phases

$$r_\varphi(t) = u_r \sin(2\pi f_r t + \theta_\varphi). \tag{1}$$

The carrier signal shared by three reference signals is defined as follows:

$$c_t(t) = \begin{cases} -4u_c\left(f_c t - k - \frac{1}{4}\right), & kT_c \le t < \left(k+\frac{1}{2}\right)T_c \\ 4u_c\left(f_c t - k - \frac{3}{4}\right), & \left(k+\frac{1}{2}\right)T_c \le t < (k+1)T_c \end{cases} \tag{2}$$

where k is a natural number; and u_c, T_c, and f_c are the amplitude, period, and frequency of the carrier signal, respectively. Based on the definition of $r_\varphi(t)$, $c_t(t)$, and the SPWM principle, the gate signal function of inverter can be derived as follows:

$$tr_\varphi(t) = \begin{cases} 1, & r_\varphi(t) - c_t(t) \ge 0 \\ 0, & r_\varphi(t) - c_t(t) < 0 \end{cases} \tag{3}$$

where φ has the values *A*, *B*, and *C* phase. $tr_\varphi(t) = 1$ stands for the ON-state of the upper switch and the OFF-state of the lower switch in phase φ. $tr_\varphi(t) = 0$ stands for the opposite state. Consequently, under normal operation, voltages on each switch are as follows:

$$\begin{cases} u_{T_x}(t) = (1 - tr_\varphi(t))\, u_{\rm dc} \\ u_{T_{x+1}}(t) = tr_\varphi(t)\, u_{\rm dc} \end{cases}, \quad x = 1, 3, 5\ . \tag{4}$$

Based on the Kirchhoff theorem and (4), the output line-to-line voltage of inverter $u_{ab}(t)$, $u_{bc}(t)$, and $u_{ca}(t)$ are obtained as shown in (6) as follows:

$$\begin{cases} u_{ab}(t) = u_{\rm dc} - u_{T_1}(t) - u_{T_4}(t) \\ u_{bc}(t) = u_{\rm dc} - u_{T_3}(t) - u_{T_6}(t) \\ u_{ca}(t) = u_{\rm dc} - u_{T_5}(t) - u_{T_2}(t) \end{cases} \tag{5}$$

$$\begin{cases} u_{ab}(t) = u_{\rm dc}\left[tr_A(t) - tr_B(t)\right] \\ u_{bc}(t) = u_{\rm dc}\left[tr_B(t) - tr_C(t)\right] \\ u_{ca}(t) = u_{\rm dc}\left[tr_C(t) - tr_A(t)\right]. \end{cases} \tag{6}$$

With the above analysis, *Proposition 1* is proposed for phase A.

Proposition 1: $u_{ab}(t)$ has periodic nonpositive and nonnegative value

$$\begin{cases} u_{ab}(t) \ge 0, & \left(k - \frac{1}{12}\right)T_r \le t < \left(k + \frac{5}{12}\right)T_r \\ u_{ab}(t) \le 0, & \left(k + \frac{5}{12}\right)T_r \le t < \left(k + \frac{11}{12}\right)T_r. \end{cases} \tag{7}$$

Proof: Based on (3), all possible values of $tr_A(t) - tr_B(t)$ are listed as follows:

$$tr_A(t) - tr_B(t) = \begin{cases} 1 & r_A(t) \ge c_t(t) > r_B(t) \\ -1 & r_A(t) < c_t(t) \le r_B(t) \\ 0 & r_A(t) \ge c_t(t)\ \&\ r_B(t) \ge c_t(t) \\ 0 & r_A(t) < c_t(t)\ \&\ r_B(t) < c_t(t). \end{cases} \tag{8}$$

It can be deduced from (8) that

$$\begin{cases} tr_A(t) - tr_B(t) \ge 0, & r_A(t) > r_B(t) \\ tr_A(t) - tr_B(t) \le 0, & r_A(t) < r_B(t). \end{cases} \tag{9}$$

By applying (9) into (6), we have

$$\begin{cases} u_{ab}(t) \geq 0, & r_A(t) - r_B(t) > 0 \\ u_{ab}(t) \leq 0, & r_A(t) - r_B(t) < 0. \end{cases} \tag{10}$$

By calculating $r_A(t) - r_B(t)$, we can obtain

$$\begin{aligned} r_A(t) - r_B(t) &= u_r \sin(2\pi f_r t) - u_r \sin\left(2\pi f_r t - \frac{2\pi}{3}\right) \\ &= \sqrt{3} u_r \sin\left(2\pi f_r t + \frac{\pi}{6}\right). \end{aligned}$$

Therefore, *Proposition 1* is proven. $u_{ab}(t)$ shifts between nonpositive and nonnegative values with the same periodicity of $r_\varphi(t)$. Using similar reasoning, *Proposition 1* can be extended to phases B and C. As a result, *Proposition 2* is proposed as follows.

Proposition 2:

$$\begin{cases} u_\varphi(t) \geq 0, & \left(k - \frac{1}{12} + \frac{\theta_\varphi}{2\pi}\right) T_r \leq t < \left(k + \frac{5}{12} + \frac{\theta_\varphi}{2\pi}\right) T_r \\ u_\varphi(t) \leq 0, & \left(k + \frac{5}{12} + \frac{\theta_\varphi}{2\pi}\right) T_r \leq t < \left(k + \frac{11}{12} + \frac{\theta_\varphi}{2\pi}\right) T_r. \end{cases} \tag{11}$$

Proposition 2 shows that the values of three-phase output line-to-line voltages are shifting between nonpositive and nonnegative. The periodicity of the shifting is the same as that of $r_\varphi(t)$, and each phase has a fixed displacement angle. To facilitate the analysis of the following, two time zones are defined in the following equation:

$$\begin{cases} t_\varphi \text{Zone}_1 = \left\{ t \middle| \left(k - \frac{1}{12} + \frac{\theta_\varphi}{2\pi}\right) T_r \leq t < \left(k + \frac{5}{12} + \frac{\theta_\varphi}{2\pi}\right) T_r \right\} \\ t_\varphi \text{Zone}_2 = \left\{ t \middle| \left(k + \frac{5}{12} + \frac{\theta_\varphi}{2\pi}\right) T_r \leq t < \left(k + \frac{11}{12} + \frac{\theta_\varphi}{2\pi}\right) T_r \right\}. \end{cases} \tag{12}$$

Now, *Proposition 2* can be rewritten as follows, where φ stands for phases *A*, *B*, and *C*. $u_\varphi(t)$ represents $u_{ab}(t)$, $u_{bc}(t)$, and $u_{ca}(t)$, respectively, for phases *A*, *B*, and *C*

$$\begin{cases} u_{ab}(t) \geq 0, & t \in t_\varphi \text{Zone}_1 \\ u_{ab}(t) \leq 0, & t \in t_\varphi \text{Zone}_2. \end{cases}$$

Based on *Proposition 2*, $u_{ab}(t)$ is taken as an example to analysis inverter's normal operation. Here, $u_{ab}(t)$ features six different states according to trigger signal and current direction. Equivalent circuits are shown in Fig. 2.

Situation 1: $tr_A(t) = tr_B(t) = 1$, which means $t \in t_A\text{Zone}_1$.

The equivalent circuit under Situation 1 is shown in Fig. 2(a). If $i_a(t) \geq 0$, current pass through T_1; else if $i_a(t) < 0$, current can only go through D_1. Therefore, no matter what the direction of $i_a(t)$ is, $u_{an}(t)$ equals to u_{dc} By the similar reasoning, $u_{bn}(t) = u_{\text{dc}}$. So, we have $u_{ab}(t) = 0$.

Situation 2: $tr_A(t) = 1$, $tr_B(t) = 0$, which means $t \in t_A\text{Zone}_1$.

This equivalent circuit is shown in Fig. 2(b), $u_{an}(t) = u_{\text{dc}}$ due to the same reason in Situation 1. If $i_b(t) > 0$, D_4 is conducted; else if $i_b(t) \leq 0$, T_4 is conducted. The point b is connected to point n either by D_4 or T_4, so we have $u_{bn}(t) = 0$ and $u_{ab}(t) = u_{\text{dc}}$.

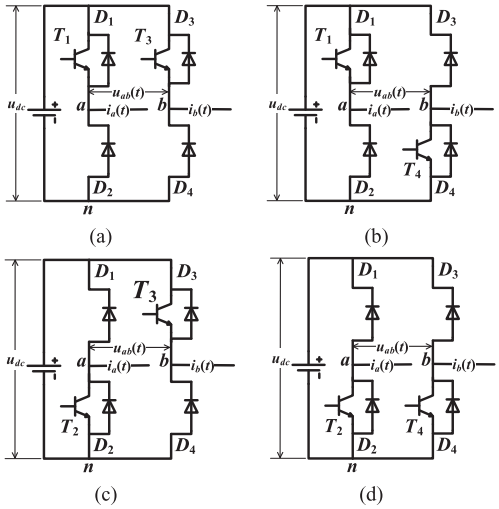

Fig. 2. Equivalent circuit of AB phase under normal operation. (a) $tr_A(t) = tr_B(t) = 1$. (b) $tr_A(t) = 1$, $tr_B(t) = 0$. (c) $tr_A(t) = 0$, $tr_B(t) = 1$. (d) $tr_A(t) = tr_B(t) = 0$.

TABLE I
LINE-TO-LINE VOLTAGE UNDER NORMAL CONDITIONS

Phase	Trigger signals			Current	Line-to-line voltage	Time zone
	$tr_A(t)$	$tr_B(t)$	$tr_C(t)$	$i_a(t)$	$u_{ab}(t)$	
A	1	1	Any	$i_a(t)>0$	0	$t_A\text{Zone}_1$
	1	1	Any	$i_a(t)=0$	0	
	1	1	Any	$i_a(t)<0$	0	
	1	0	Any	$i_a(t)>0$	u_{dc}	
	1	0	Any	$i_a(t)=0$	u_{dc}	
	1	0	Any	$i_a(t)<0$	u_{dc}	
A	0	1	Any	$i_a(t)>0$	$-u_{dc}$	$t_A\text{Zone}_2$
	0	1	Any	$i_a(t)=0$	$-u_{dc}$	
	0	1	Any	$i_a(t)<0$	$-u_{dc}$	
	0	0	Any	$i_a(t)>0$	0	
	0	0	Any	$i_a(t)=0$	0	
	0	0	Any	$i_a(t)<0$	0	

Situation 3: $tr_A(t) = 0$, $tr_B(t) = 1$, which means $t \in t_A\text{Zone}_2$.

The equivalent circuit is shown in Fig. 2(c). T_2 is conducted when $i_a(t) \leq 0$, and D_2 is conducted when $i_a(t) > 0$. Both situations will cause $u_{an}(t)$ equals to zero. $u_{bn}(t) = u_{\text{dc}}$ due to the same reason in Situation 1. So, we have $u_{ab}(t) = u_{\text{dc}}$.

Situation 4: $tr_A(t) = tr_B(t) = 0$, which means $t \in t_A\text{Zone}_2$.

In this situation, with any direction of $i_a(t)$ and $i_b(t)$ we have $u_{an}(t) = u_{bn}(t) = 0$. So $u_{ab}(t) = 0$.

By summarizing the above analysis, $u_{ab}(t)$ and other parameters can be concluded, as shown in Table I. $u_{bc}(t)$ and $u_{ca}(t)$ can also be inferred by the same way, which will not be discussed in detail here.

B. Faulty Operation of Inverter

The operation of inverter under single switch open-circuit fault is present in this section by taking T_1 open-circuit fault as

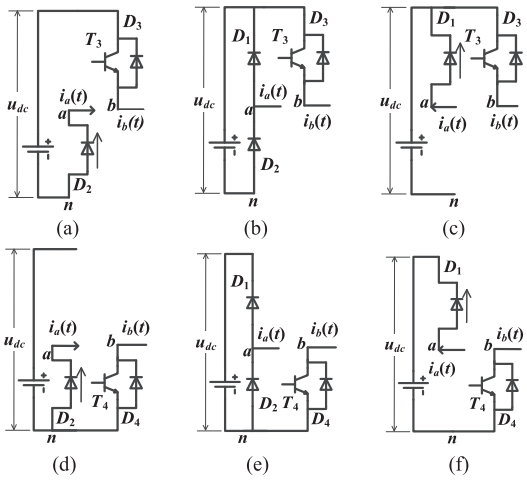

Fig. 3. Topology of AB phase under T_1 open-circuit fault. (a) $i_a(t) > 0,\ tr_B(t) = 1$. (b) $i_a(t) = 0,\ tr_B(t) = 1$. (c) $i_a(t) < 0,\ tr_B(t) = 1$. (d) $i_a(t) > 0,\ tr_B(t) = 0$. (e) $i_a(t) = 0,\ tr_B(t) = 1$. (f) $i_a(t) < 0,\ tr_B(t) = 1$.

an example. If T_1 open-circuit fault occurs while $tr_A(t) = 0$, the behavior of inverter is identical to its normal operation. Inverter output is different from that of normal operation only if T_1 open-circuit fault happens during $tr_A(t) = 1$. $tr_A(t) = 1$ leads to $tr_A(t) - tr_B(t) \geq 0$, which is above defined as $t_A\text{Zone}_1$ in *Proposition 2*. Consequently, only T_1 open-circuit fault in $t_A\text{Zone}_1$ is analyzed here. Based on (6), $u_{ab}(t)$ is affected by $tr_B(t)$ and $i_a(t)$. Thus, the operation under T_1 open-circuit fault is divided into six situations; the equivalent circuits and current direction for each situation are shown in Fig. 3.

Situation 1: $i_a(t) > 0, tr_B(t) = 1$

$i_a(t)$ goes through D_2, thus $u_{an}(t) = 0$. If $i_b(t) > 0$, T_3 is conducted; else if $i_b(t) < 0$, D_3 is conducted. So, $u_{bn}(t) = u_{\text{dc}}$, and $u_{ab}(t) = -u_{\text{dc}}$.

Situation 2: $i_a(t) = 0, tr_B(t) = 1$

D_1 and D_2 are cutoff in this situation. Thus, $u_{an}(t) = 1/2u_{\text{dc}}$; $u_{bn}(t)$ equals to u_{dc} no matter what direction $i_b(t)$ is. So, we have $u_{ab}(t) = -1/2u_{\text{dc}}$.

Situation 3: $i_a(t) < 0, tr_B(t) = 1$

$i_a(t)$ goes through D_1, thus $u_{an}(t) = u_{\text{dc}}$. $u_{bn}(t) = u_{\text{dc}}$ because either D_3 or T_3 is conducted. So, we have $u_{ab}(t) = 0$.

Situation 4: $i_a(t) > 0, tr_B(t) = 0$

$i_a(t)$ goes through D_2, thus $u_{an}(t) = 0$; $u_{bn}(t) = 0$ because $i_b(t)$ goes through T_4 or D_4; so, we have $u_{ab}(t) = 0$.

Situation 5: $i_a(t) = 0, tr_B(t) = 0$

D_1 and D_2 are not conducted, $u_{an}(t) = 1/2u_{\text{dc}}$. $u_{bn}(t) = 0$ because T_4 or D_4 is conducted. So, we have $u_{ab}(t) = 1/2u_{\text{dc}}$.

Situation 6: $i_a(t) < 0, tr_B(t) = 0$

$i_a(t)$ goes through D_1, thus $u_{an}(t) = u_{\text{dc}}$. $u_{bn}(t) = 0$ because either D_4 or T_4 is conducted; so, we have $u_{ab}(t) = u_{\text{dc}}$.

Same reasoning can be applied to T_2 open-circuit fault. Table II presents the inverter states of T_1 and T_2 open-circuit faults occur in $t_A\text{Zone}_1$ and $t_A\text{Zone}_2$, respectively. All single switch open-circuit faults can be analyzed by the same way, the results are similar but only different in time zone.

TABLE II
LINE-TO-LINE VOLTAGE UNDER FAULT CONDITION

Phase	Faulty part	Trigger signals		Current $i_a(t)$	Line-to-line voltage	Time zone
		$tr_A(t)$	$tr_B(t)$		$u_{ab}(t)$	
A	T_1	1	1	$i_a(t)>0$	$-u_{dc}$	$t_A\text{Zone}_1$
		1	1	$i_a(t)=0$	$-1/2\ u_{dc}$	
		1	1	$i_a(t)<0$	0	
		1	0	$i_a(t)>0$	0	
		1	0	$i_a(t)=0$	$1/2\ u_{dc}$	
		1	0	$i_a(t)<0$	u_{dc}	
A	T_2	0	1	$i_a(t)>0$	$-u_{dc}$	$t_A\text{Zone}_2$
		0	1	$i_a(t)=0$	$-1/2u_{dc}$	
		0	1	$i_a(t)<0$	0	
		0	0	$i_a(t)>0$	0	
		0	0	$i_a(t)=0$	$1/2u_{dc}$	
		0	0	$i_a(t)<0$	u_{dc}	

IV. PROPOSED FAULT DIAGNOSIS METHOD

The analysis above shows that the single switch open-circuit fault can make output line-to-line voltage disobey *Proposition 2*, which can provide enough information for fault locating. Take T_1 and T_2 open-circuit faults as examples, based on the above analysis, it is easy to find out that the inverter is operating normally except two situations. The first situation is that, T_1 open-circuit fault happens in $t_A\text{Zone}_1$ and meanwhile $i_a(t) \geq 0$, which will causes the negative voltage of $u_{ab}(t)$ in $t_A\text{Zone}_1$. The second situation is that, T_2 open-circuit fault happens in $t_A\text{Zone}_2$ and meanwhile $i_a(t) \leq 0$, which will causes the positive voltage of $u_{ab}(t)$ in $t_A\text{Zone}_2$. Moreover, the output line-to-line voltage still shows a certain periodicity after open-circuit fault occurs. By utilizing these features, faulty switch can be located.

A. Preprocess of Diagnosis Eigenvalue

According to *Proposition 2* and Table II, the output line-to-line voltage is only deviated from its normal state in two particular situations. One of the situations is that the output line-to-line voltage will become negative in $t_A\text{Zone}_1$ when the upper switch open-circuit fault occurs. Another situation is that the output line-to-line voltage will appear positive value in $t_A\text{Zone}_2$ when the lower switch open-circuit fault occurs. Therefore, a diagnosis eigenvalue preprocessing equation is defined as follows to remove faulty-state-irrelevant information:

$$u_m^{\text{upper}}(t) = \begin{cases} u_{\text{dc}} & u_n(t) < -u_{TH} \\ 0 & u_n(t) \geq -u_{TH} \end{cases}$$
$$u_m^{\text{lower}}(t) = \begin{cases} u_{\text{dc}} & u_n(t) > u_{TH} \\ 0 & u_n(t) \leq u_{TH} \end{cases} \quad (13)$$

where $m = 1, 2, 3$; $n = 1, 2, 3$; u_n represents $u_{ab}(t)$, $u_{bc}(t)$, and $u_{ca}(t)$ for $n = 1, 2, 3$, respectively. $u_m^{\text{upper}}(t)$ and $u_m^{\text{lower}}(t)$ are the preprocessed open-circuit fault characteristic variables of the upper and lower power switches in phase m, respectively. u_{TH} is a constant. The restriction on the choices of u_{TH} is relatively loose because the amplitude of the output line-to-line

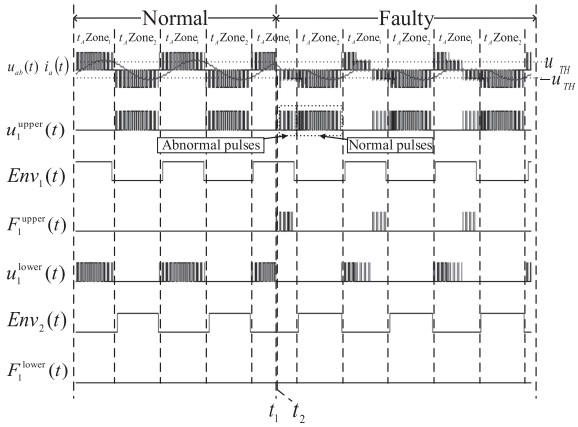

Fig. 4. Timing of fault diagnosis process for T_1 open circuit.

voltage is not critical to the proposed method. Therefore, u_{TH} can be any value between 0 and $1/2u_{\rm dc}$. Here, $u_{TH} = 250$ V with the consideration of noisy, interference, and margin.

B. Preprocess of Diagnosis Eigenvalue

The preprocessed diagnosis eigenvalues under normal and abnormal states are different positive pulses emerge on $u_m^{\rm upper}(t)$ within $t_A{\rm Zone}_1$ when the upper switch open-circuit fault occurs. This difference is tagged in Fig. 4. It can be concluded that, preprocessed diagnosis eigenvalues have two kinds of pulses, which are normal and abnormal pulses. The envelope function is proposed as shown in (14) to classify the pulses

$$\begin{aligned} {\rm Env}_{2n-1}(t) &= \begin{cases} u_{\rm dc}, & t \in t_\phi{\rm Zone}_1 \\ 0, & {\rm Env}_{2n-1}(t) \neq u_{\rm dc} \end{cases} \\ {\rm Env}_{2n}(t) &= \begin{cases} u_{\rm dc}, & t \in t_\phi{\rm Zone}_2 \\ 0, & {\rm Env}_{2n}(t) \neq u_{\rm dc} \end{cases} \end{aligned} \tag{14}$$

where $n = 1, 2, 3$. Equation (14) defines six envelope functions for $T_1 - T_6$ under open-circuit fault, respectively.

C. Classification and Identification of the Faulty State

The open-circuit fault is located by comparing the preprocessed diagnosis eigenvalue and its envelope line. The fault diagnosis function is defined in the following. A fault is detected when the function has a nonzero value

$$F_n^{\rm upper} = u_n^{\rm upper}(t) \ \& \ {\rm Env}_{2n-1}(t) \tag{15}$$

$$F_n^{\rm lower} = u_n^{\rm lower}(t) \ \& \ {\rm Env}_{2n}(t). \tag{16}$$

Assuming T_1 open-circuit fault occurs at t_1, the proposed method is illustrated in the following. The analysis process is divided into two steps of normal and faulty state. The timing of the fault diagnosis process for T_1 open-circuit fault is shown in Fig. 4.

Step 1) Under inverter normal state ($t < t_1$)

$\theta_A = 0$ and T_1 is the upper switch, thus the characteristic variable and envelope function are obtained as follows:

$$u_1^{\rm upper}(t) = \begin{cases} u_{\rm dc} & u_{\rm ab}(t) < -u_{TH} \\ 0 & u_{ab}(t) \geq -u_{TH} \end{cases} \tag{17}$$

$${\rm Env}_1(t) = \begin{cases} u_{\rm dc}, & t \in t_\varphi{\rm Zone}_1 \\ 0, & {\rm Env}_1(t) \neq u_{\rm dc}. \end{cases} \tag{18}$$

From Table I, we have

$$u_{ab}(t) = \begin{cases} u_{\rm dc} \text{ or } 0, & t \in t_A{\rm Zone}_1 \\ -u_{\rm dc} \text{ or } 0, & t \in t_A{\rm Zone}_2. \end{cases} \tag{19}$$

By replacing $u_{ab}(t)$ in (17), we have

$$u_1^{\rm upper}(t) = \begin{cases} 0 & t \in t_A{\rm Zone}_1 \\ u_{\rm dc} \text{ or } 0 & t \in t_A{\rm Zone}_2. \end{cases} \tag{20}$$

Applying $u_1^{\rm upper}(t)$ and $Env_1(t)$ in (15) gives

$$F_1^{\rm upper}(t) = 0 \ \ \forall t. \tag{21}$$

Similarly, it can be inferred that

$$F_1^{\rm lower}(t) = 0 \ \ \forall t.$$

There is no false alarm under inverter normal state.

Step 2) Under inverter fault state ($t > t_1$)

From Table II, we have

$$u_{ab}(t) = \begin{cases} u_{\rm dc} \ \ or \ -u_{\rm dc} \ \text{or} \ 0, & t \in t_A{\rm Zone}_1 \\ -u_{\rm dc} \ or \ 0, & t \in t_A{\rm Zone}_2. \end{cases} \tag{22}$$

Applying $u_{ab}(t)$ in (17) gives

$$u_1^{\rm upper}(t) = \begin{cases} u_{\rm dc} \text{ or } 0, & t \in t_A{\rm Zone}_1 \\ u_{\rm dc} \text{ or } 0, & t \in t_A{\rm Zone}_2. \end{cases} \tag{23}$$

By substituting $u_1^{\rm upper}(t)$ and ${\rm Env}_1(t)$ into (15), we have

$$F_1^{\rm upper}(t) = \begin{cases} u_{\rm dc} \text{ or } 0, & t \in t_A{\rm Zone}_1 \\ 0, & t \in t_A{\rm Zone}_2. \end{cases} \tag{24}$$

Thus, the open-circuit fault happened in T_1 is confirmed. Meanwhile, similar reasoning is applied to preprocessed diagnosis eigenvalue, envelope, and fault diagnosis function of T_2, and $F_1^{\rm lower}(t)$ is obtained as

$$F_1^{\rm lower}(t) = 0 \ \ \forall t. \tag{25}$$

There is no false alarm. Open-circuit fault on any other switches can be handled in the same way using (13)–(16).

V. Effectiveness of the Proposed Method

A. Influence of Load and Modulation Index Changing

The load changing normally has great influence over output current. Meanwhile, the output voltage is constantly regulated by the control system. There are only few ripples in output voltage when load changes. Ripples of output voltage are only reflected on the PWM duty cycle of the output line-to-line voltage. The modulation index variation has similar effects on the proposed method and it only affects the PWM duty cycle. Consequently, the load and modulation index changing will not affect the effectiveness of Proposition 2 (Tables I and II). The proposed method is independent from the load changing as well as the modulation index changing.

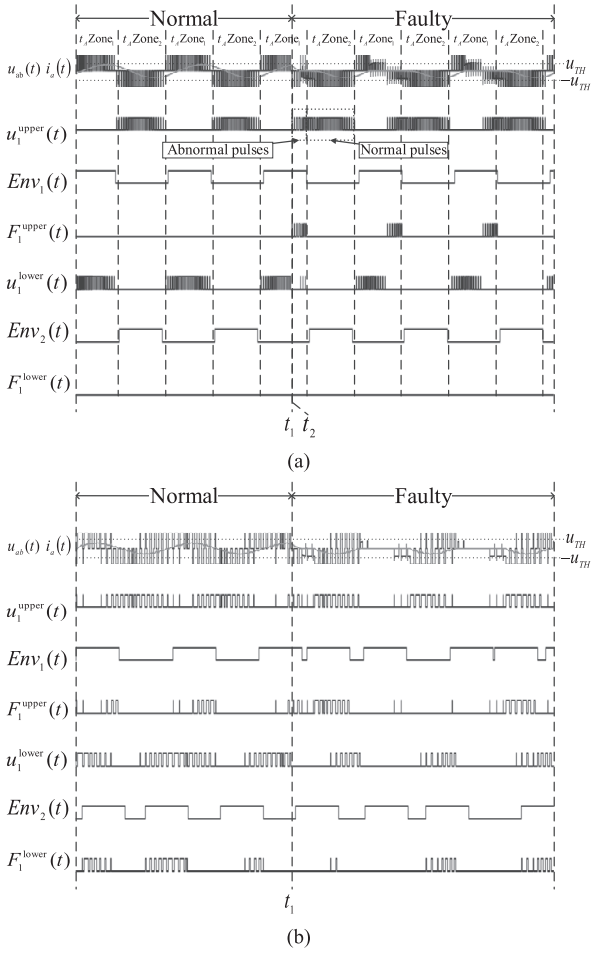

Fig. 5. Influence of different control strategies. (a) Diagnosis process for SVPWM-based inverter. (b) Diagnosis process for hysteresis current PWM-based inverter.

B. Influence of Different Control Strategies

The proposed method is built based on the periodicity of nonpositive and nonnegative value on output line-to-line voltage. Thus, as long as the inverter output voltages have the feature of periodic nonpositive and nonnegative, this method is valid no matter what control strategy is adopted by the inverter.

Take SVPWM and hysteresis current PWM as two examples and the simulation results are shown in Fig. 5. Assuming T_1 open-circuit fault happens at t_1. The output voltage of SVPWM-based inverter meets the periodic nonpositive and nonnegative conditions, thus the T_1 open-circuit fault can be located at t_2, as shown in Fig. 5(a).

On the contrary, the hysteresis current PWM-based inverter does not produce the periodic nonpositive and nonnegative output voltage, the proposed method cannot work properly on these kinds of inverters. The waveforms of the proposed method applying on the hysteresis current PWM-based inverter are shown in Fig. 5(b). The diagnosis method for this kind of inverters will be our next research work.

Furthermore, if the output voltage frequency or the carrier frequency of SPWM is higher, the diagnosis speed will be increased. Diagnosis accuracy will not be affected by PWM frequency.

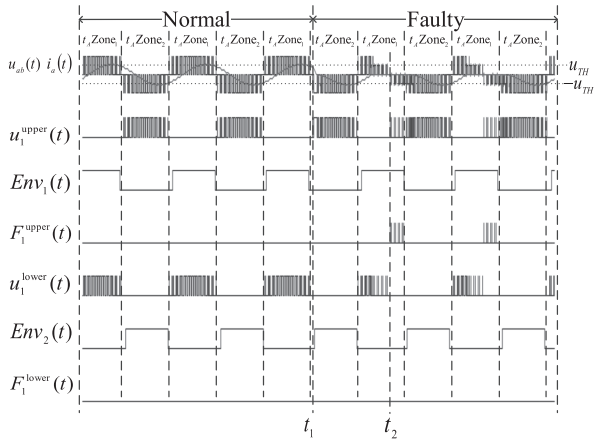

Fig. 6. Diagnosis delay of T_1 open-circuit under worst situation.

C. Influence of Fault Timing, Current Displacement Factor, and Current Distortion

The open-circuit fault occurring time t_1 and the output current displacement factor have influence on the diagnosis speed of the proposed method. Take T_1 open-circuit fault at t_1 as an example. When $t_1 \in t_A\text{Zone}_1$ and $i_a(t) \geq 0$, the open-circuit fault will affect output voltage immediately. The time interval between t_1 and t_2 is no more than one carrier period, as shown in Fig. 4. However, if the open-circuit fault occurs in $t_A\text{Zone}_2$ or when $i_a(t) \leq 0$, the output voltage stays normal, and the inverter works normally. After the inverter goes into $t_A\text{Zone}_1$ and $i_a(t)$ goes to above zero, the fault is diagnosed in one carrier period, as shown in Fig. 6. It can be concluded that, the smaller the output current displacement factor is, the wider the range of instant diagnosis is, due to a wider overlap area of $t_A\text{Zone}_1$ and $i_a(t) \geq 0$.

The influence of current distortion factor is also incarnated in $i_a(t)$. The distortion may cause $i_a(t)$ cross zero randomly near its original zero-cross point, if the zero cross happens in $t_A\text{Zone}_1$, the fault characteristics may emerge synchronously. The fault will be diagnosed once the characteristics emerge.

There is another possibility, in which the fault occurring time t_1 is too close to the border of the time zone $t_A\text{Zone}_1$ and $t_A\text{Zone}_2$. In this circumstance, the diagnosis speed is decided by the fault diagnosis circuit parameters. In our prototype, if t_1 is within 0.1-ms range of the time zone border, the fault will have to wait additional half-working-cycle to be located.

Notice that the power switch open-circuit fault usually happens under high-voltage and large current situations. However, when $i_a(t) \leq 0$ or in $t_A\text{Zone}_2$. T_1 is kept off and the current will go through D_1 instead. Thus, the possibilities of T_1 open-circuit fault under $t_1 \in t_A\text{Zone}_2$ or $i_a(t) \leq 0$ conditions are relatively low. The above discussion is only to make a comprehensive assessment of the proposed method.

VI. Experimental Result

An inverter open-circuit fault test bed is built to verify the effectiveness and robustness of the proposed method. The block diagram of the test bed is shown in Fig. 7.

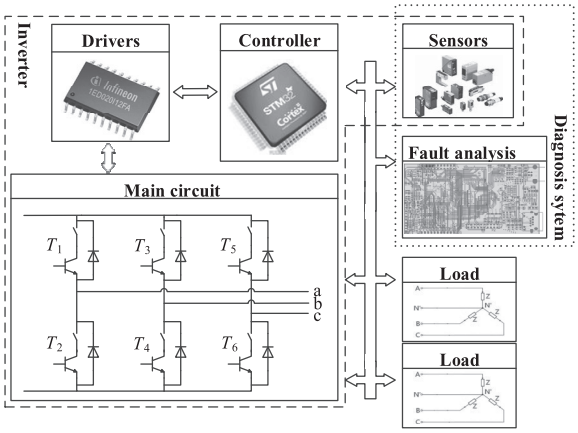

Fig. 7. Block diagram of the experimental setup.

TABLE III
KEY PARAMETERS OF THE PROTOTYPE

Parameters	Value	Parameters	Value
T_1-T_6	IKW40N120T2	Controller	f_r=50 Hz
Trigger IC	1ED020I12FA		f_c=4.5 kHz
Load	4.5 kW × 2		Modulation index is 0.8
Input voltage	600 VDC	Diagnosis system	u_{TH}=250 V
Output voltage	Three phases 380 VAC		

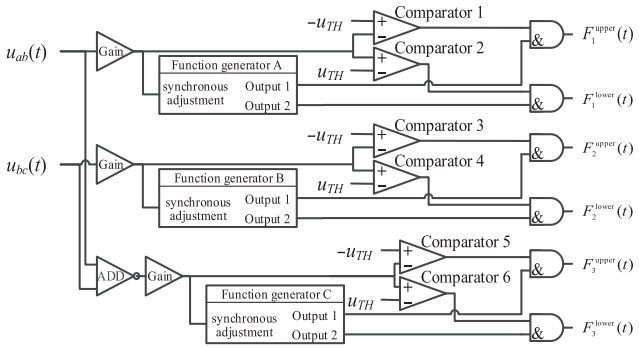

Fig. 8. Block diagram of the fault diagnosis system.

Contactors are added to each leg of the test bed to imitate the open-circuit fault. Because IKW series IGBTs have body diodes, two IGBTs are installed in each leg, one of the IGBT is connected in series with a contactor. Another IGBT is used as freewheeling diodes for that leg, as shown in Fig. 7. The key parameters of the test bed are listed in Table III.

The block diagram of the fault diagnosis system is shown in Fig. 8, where the function generators are designed to produce the envelope line defined in (14), the function generators have built-in synchronous adjustment function that keeps the envelope line synchronized with the measured output voltage. Comparators are utilized to implement (13) and preprocess the diagnosis eigenvalue.

Because the implementation of the proposed method does not rely on the accurate amplitude of the output line-to-line voltage, $u_{ab}(t)$ and $u_{bc}(t)$ can be collected by the inherent sensors if the inverter has. Or, they can be introduced to the diagnosis system

TABLE IV
ORDER OF DIAGNOSIS SIGNAL AFTER OPEN-CIRCUIT FAULT

Faulty switch	First-appeared	Later appeared
T_1	$F_1^{upper}(t)$	$F_3^{lower}(t)$
T_2	$F_1^{lower}(t)$	$F_3^{upper}(t)$
T_3	$F_2^{upper}(t)$	$F_1^{lower}(t)$
T_4	$F_2^{lower}(t)$	$F_1^{upper}(t)$
T_5	$F_3^{upper}(t)$	$F_2^{lower}(t)$
T_6	$F_3^{lower}(t)$	$F_2^{upper}(t)$

with simple isolated bleeder circuits, which can also preserve enough periodic property on the introduced voltages for fault diagnosis. There are abundant low-cost high-speed operational amplifier and optocoupler integrated chips in the market, so the proposed fault diagnosis system can be cheap and need no extra sensors. $u_{ca}(t)$ is obtained by reversing the sign of a sum of $u_{ab}(t)$ and $u_{bc}(t)$. $F_m^{\text{upper}}(t)$ and $F_m^{\text{lower}}(t)$ are the fault location signal generated by the fault analysis system. $F_m^{\text{upper}}(t)$ and $F_m^{\text{lower}}(t)$ are equal to zero when inverter is healthy. But when an open-circuit fault happens, the corresponding $F_m^{\text{upper}}(t)$ and $F_m^{\text{lower}}(t)$ can produce pulses within one carrier period to identify the open-circuit fault and locate the faulty switch.

Note that T_1 open-circuit fault will cause distortion in not only $u_{ab}(t)$, but also $u_{ca}(t)$. $F_3^{\text{lower}}(t)$ will generate pulses later than $F_1^{\text{lower}}(t)$. In the practical fault diagnosis system, the first appearing pulses are admitted and the later pulses are used as a supplement. The diagnosis pulses of each switch open-circuit fault are listed in Table IV in sequence.

The waveforms of T_1 open-circuit fault are shown in Fig. 9. The fault occurs at t_1 in $t_A\text{Zone}_1$ while $i_a(t) < 0$. Thus, the output voltage is not affected instantly. The fault feature does not appear until $i_a(t) \geq 0$ at t_2. This situation is rare in practical tests. The situation is analyzed here to prove the comprehensiveness of the proposed method. The fault is simulated by breaking off the contactor, which is connected in series to T_x. After output line-to-line voltage meets the threshold u_{TH} of (13) at t_3, and the faulty switch is located.

It is concluded from Fig. 9 that the open-circuit fault of T_1 can be diagnosed in half an inverter working cycle, and there is no false alarm in $F_2^{\text{upper}}(t)$ and $F_2^{\text{lower}}(t)$. $F_3^{\text{lower}}(t)$ also obeys the rules of Table IV.

Fig. 10 shows the influence of load changing on the proposed method. The load is stepped from 4.5 to 9 kW at t_1, and T_2 open-circuit occurs at t_2.

The change of load causes rapid change of phase current, its peak value is almost doubled. The duty cycle of output voltage is changed, but not the envelope line. Consequently, the proposed method is independent to load changing and suitable for applications with large and fast load changing, such as the onboard inverter of passenger train. In this test, T_2 open-circuit fault happened in $t_A\text{Zone}_2$, but $i_a(t)$ is above zero at that time. Therefore, the fault feature will not appear until t_3. Then, faulty switch is located at t_4. In fact, the phenomenon of fault feature lags in both Figs. 9 and 10 are rare, because the current will go through D_2 instead of T_2 if $i_a(t) \geq 0$. So, T_2 is bypassed and has low possibility of open-circuit fault. For the same reason, when $i_a(t) < 0$, T_1 is relatively safe. The above tests are implemented to verify the proposed method comprehensively.

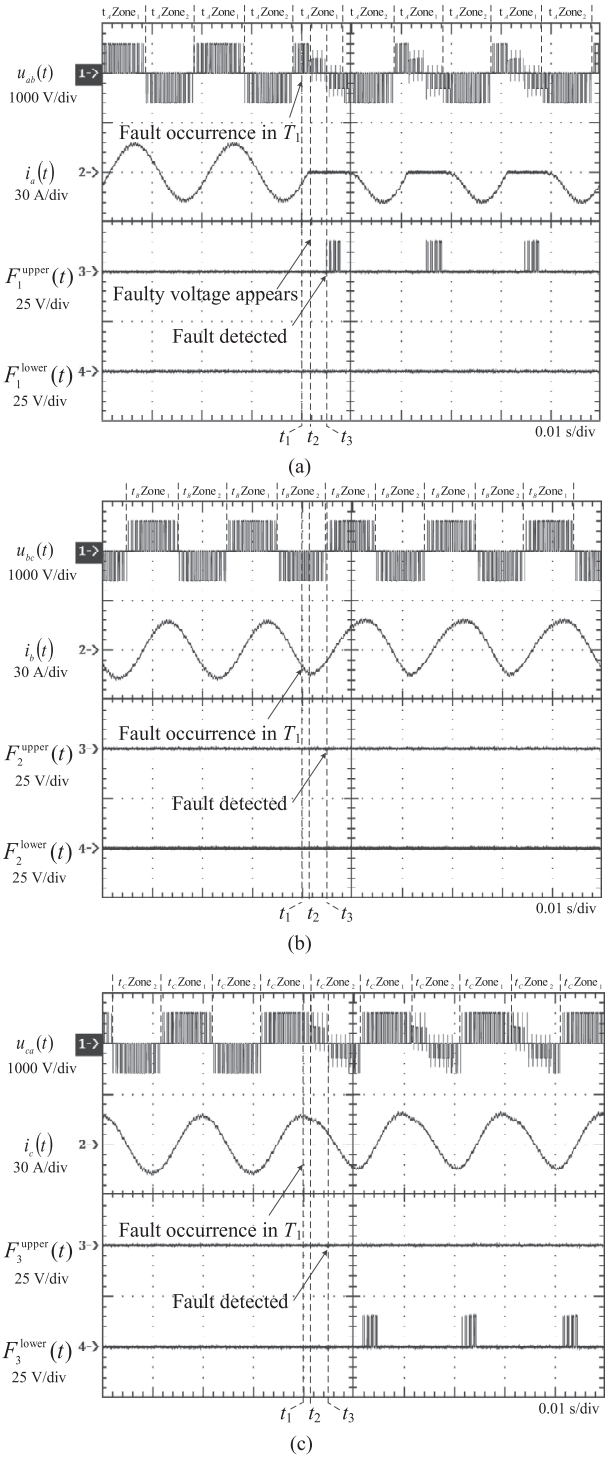

Fig. 9. Fault diagnosis waveforms of T_1 open-circuit. (a) Waveforms of $u_{ab}(t)$ and $F_1^{\mathrm{x}}(t)$. (b) Waveforms of $u_{bc}(t)$ and $F_2^{\mathrm{x}}(t)$. (c) Waveforms of $u_{ca}(t)$ and $F_3^{\mathrm{x}}(t)$.

Fig. 11 shows the influence of different carrier frequency on the proposed method. The carrier frequency is increased to 22.5 kHz in this test. T_4 open-circuit fault occurs at t_1. Because the carrier frequency increase only affects the switching frequency of T_x, the period and amplitude of output voltage and its envelope line stay intact. The effectiveness of the proposed method is retained. On the other hand, the diagnosis time of

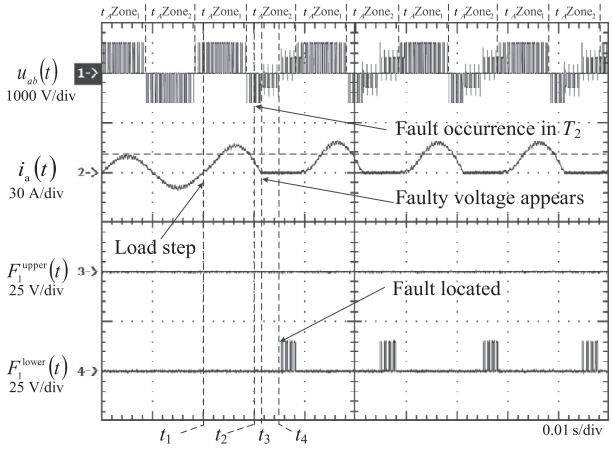

Fig. 10. Influence of load changing.

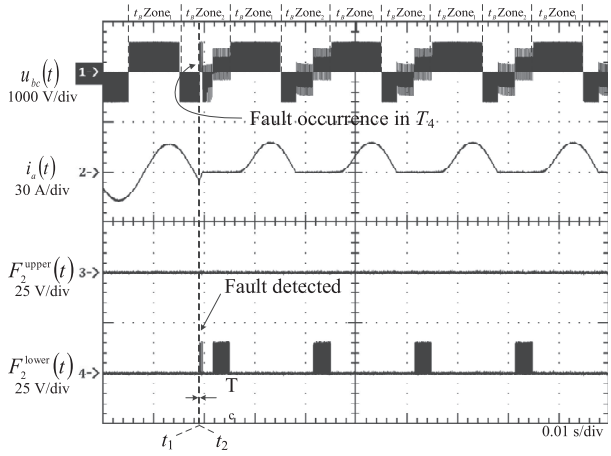

Fig. 11. T_c's influence on the proposed method.

the proposed method is even shortened by the higher switching frequency. Another difference between the situation of Figs. 10 and 11 is that T_4 open-circuit fault happens in $t_B\mathrm{Zone}_2$ and $i_b(t) \leq 0$. Therefore, the output voltage is affected immediately and the fault is located in one carrier period.

VII. Conclusion

In this paper, the features of output line-to-line voltage were analyzed under normal and single switch open-circuit fault conditions. An output line-to-line voltage envelope-based diagnosis method was proposed. This method only employs output voltage as the diagnosis eigenvalue to extract the fault features; neither the inverter control signal nor the complex hardware is needed. Within the rated operating range of inverter, the robustness of the proposed method under various loading conditions is validated owing to the property of the output voltage. Regardless of control strategy, the presented technique has strong adaptability as long as the output voltage is periodic nonpositive and nonnegative. The effectiveness of the proposed method was verified on the experimental bench that is built to simulate the normal and open-circuit fault states of the inverter. The open-circuit fault is usually located in one carrier period. Even in the worst situation, the fault can be diagnosed in half

an inverter working cycle. Research and report of this method's application on multiswitches' open-circuit faults are planned in a subsequent paper.

References

[1] H. Ma and L. G. Wang, "Fault diagnosis and failure prediction of aluminum electrolytic capacitors in power electronic converters," in *Proc. 31st Annu. Conf. IEEE Ind. Electron. Soc.*, 2005, pp. 842–847.

[2] Y. Yu, T. Zhou, and M. G. Zhu, "Fault diagnosis and life prediction of dc-link aluminum electrolytic capacitors used in three-phase ac/dc/ac converters," in *Proc. 2nd Int. Conf. Instrum. Meas. Comput. Commun. Control*, 2012, pp. 825–830.

[3] X. S. Pu, T. H. Nguyen, and D. C. Lee, "Fault diagnosis of dc-link capacitors in three-phase ac/dc PWM converters by online estimation of equivalent series resistance," *IEEE Trans. Ind. Electron.*, vol. 60, no. 9, pp. 4118–4127, Sep. 2013.

[4] A. Braham, A. Lahyani, and P. Venet, "Recent developments in fault detection and power loss estimation of electrolytic capacitors," *IEEE Trans. Power Electron.*, vol. 25, no. 1, pp. 33–43, Jan. 2010.

[5] A. E. Ginart, D. W. Brown, and P. W. Kalgren, "Online ringing characterization as a diagnostic technique for IGBTs in power drives," *IEEE Trans. Instrum. Meas.*, vol. 58, no. 7, pp. 2290–2299, Jul. 2009.

[6] B. Ji, V. Pickert, W. Cao, and B. Zahawi, "In situ diagnostics and prognostics of wire bonding faults in IGBT modules for electric vehicle drives," *IEEE Trans. Power Electron.*, vol. 28, no. 12, pp. 5568–5578, Dec. 2013.

[7] R. L. de Araujo Ribeiro, C. B. Jacobina, E. R. C. Silva, and A. M. N. Lima, "Fault detection of open-switch damage in voltage-fed PWM motor drive systems," *IEEE Trans. Power Electron.*, vol. 18, no. 2, pp. 587–593, Mar. 2003.

[8] M. Alavi, D. Wang, and M. Luo, "Short-circuit fault diagnosis for three-phase inverters based on voltage-space patterns," *IEEE Trans. Ind. Electron.*, vol. 61, no. 10, pp. 5558–5570, Oct. 2014.

[9] J. O. Estima and A. J. Marques Cardoso, "A new algorithm for real-time multiple open-circuit fault diagnosis in voltage-fed PWM motor drives by the reference current errors," *IEEE Trans. Ind. Electron.*, vol. 60, no. 8, pp. 3496–3506, Aug. 2013.

[10] I. Jlassi, J. O. Estima, E. Khil, S. Khojet, N. M. Bellaaj, and A. J. Marques Cardoso, "Multiple open-circuit faults diagnosis in back-to-back converters of PMSG drives for wind turbine systems," *IEEE Trans. Power Electron.*, vol. 30, no. 5, pp. 2689–2703, May 2015.

[11] M. Trabelsi, M. Boussak, and M. Gossa, "PWM-switching pattern-based diagnosis scheme for single and multiple open-switch damages in VSI-fed induction motor drives," *ISA Trans.*, vol. 51, no. 2, pp. 333–344, 2012.

[12] Q. Wang, Y. R. Wang, and Z. F. Zhang, "A diagnosis method for inverter open-circuit faults of brushless dc motor driver systems," *Proc. CSEE*, vol. 33, no. 24, pp. 114–122, Aug. 2013.

[13] B. J. Jiang and Q. T. An, "A novel diagnostic technique for open-switch faults of inverters based on operating mode analysis," *Proc. CSEE*, vol. 32, no. 24, pp. 30–39, Aug. 2012.

[14] M. Shahbazi, E. Jamshidpour, and P. Poure, "Open- and short-circuit switch fault diagnosis for non-isolated dc–dc converters using field programmable gate array," *IEEE Trans. Ind. Electron.*, vol. 60, no. 9, pp. 4136–4147, Sep. 2013.

[15] M. A. F. Nuno, O. E. Jorge, and J. M. C. António, "A voltage-based approach without extra hardware for open-circuit fault diagnosis in closed-loop PWM ac regenerative drives," *IEEE Trans. Ind. Electron.*, vol. 61, no. 9, pp. 4960–4971, Sep. 2014.

[16] C. Brunson, L. Empringham, L. De Lillo, P. Wheeler, and J. Clare, "Open-circuit fault detection and diagnosis in matrix converters," *IEEE Trans. Power Electron.*, vol. 30, no. 5, pp. 2840–2848, May 2015.

[17] F. Meinguet, P. Sandulescu, X. Kestelyn, and E. Semail, "A method for fault detection and isolation based on the processing of multiple diagnostic indices: Application to inverter faults in ac drives," *IEEE Trans. Veh. Technol.*, vol. 62, no. 3, pp. 995–1010, Mar. 2013.

[18] W. Sleszynski, J. Nieznanski, and A. Cichowski, "Open-transistor fault diagnostics in voltage-source inverters by analyzing the load currents," *IEEE Trans. Ind. Electron.*, vol. 56, no. 11, pp. 4681–4688, Nov. 2009.

[19] S.-M. Jung, J.-S. Park, H.-W. Kim, K.-Y. Cho, and M.-J. Youn, "An MRAS-based diagnosis of open-circuit fault in PWM voltage-source inverters for PM synchronous motor drive systems," *IEEE Trans. Power Electron.*, vol. 28, no. 5, pp. 2514–2527, May 2013.

[20] U.-M. Choi, H.-G. Jeong, and K.-B. Lee, "Method for detecting an open-switch fault in a grid-connected NPC inverter system," *IEEE Trans. Power Electron.*, vol. 27, no. 6, pp. 2726–2740, Jun. 2012.

[21] A. B. Youssef, S. K. El Khil, and I. Slama-Belkhodja, "State observer-based sensor fault detection and isolation, and fault tolerant control of a single-phase PWM rectifier for electric railway traction," *IEEE Trans. Power Electron.*, vol. 28, no. 12, pp. 5842–5854, Dec. 2013.

[22] Y. Song and B. Wang, "Survey on reliability of power electronic systems," *IEEE Trans. Power Electron.*, vol. 28, no. 1, pp. 591–605, Jan. 2013.

[23] R. L. A. Ribeiro, C. B. Jacobina, and E. R. C. Silva, "Fault-tolerant voltage-fed PWM inverter ac motor drive systems," *IEEE Trans. Ind. Electron.*, vol. 51, no. 2, pp. 439–446, Apr. 2004.

[24] B. Lu and S. K. Sharma, "A literature review of IGBT fault diagnostic and protection methods for power inverters," *IEEE Trans. Ind. Appl.*, vol. 45, no. 5, pp. 1770–1777, Sep./Oct. 2009.

[25] F. Abrahamsen, F. Blaabjerg, and K. Ries, "Fuse protection of IGBTs against rupture," in *Proc. IEEE Nordic Workshop Power Ind. Electron.*, 2004, pp. 611–615.

[26] F. Iov, F. Blaabjerg, and K. Ries, "IGBT module rupture categorization and testing," in *Proc. 5th Int. Power Electron. Conf.*, 2001, pp. 1259–1266.

Cheng Shu was born in Changsha, China, in 1981. He received the B.E. degree in automation from East China University of Science and Technology, Shanghai, China, in 2003, and the M.S. and Ph.D. degrees in electrical engineering from Central South University (CSU), Changsha, China, in 2006 and 2011, respectively.

Since 2007, he has been a Permanent Researcher with the Institute of Rail Transport and Electric Traction Technology, CSU, and a Lecturer with the School of Traffic and Transportation Engineering, CSU. His research interests include fault diagnosis and fault-tolerant control of electrical drivers and electric traction control technology.

Chen Ya-Ting received the B.E. degree in automation from Central South University (CSU), Changsha, China, in 2011. She is currently working toward the Ph.D. degree in traffic equipment and information engineering at the Institute of Rail Transport and Electric Traction Technology, CSU.

Since 2014, she has been a joint-training Ph.D. Student with the University of Pittsburgh, Pittsburgh, PA, USA. Her research interests include fault diagnosis of locomotive inverters, and the reliability and lifetime prediction of IGBT modules.

Yu Tian-Jian received the B.E. degree in automation from Central South University (CSU), Changsha, China, in 2011. He is currently working toward the Ph.D. degree in traffic equipment and information engineering at the Institute of Rail Transport and Electric Traction Technology, CSU.

Since 2014, he has been a Visiting Ph.D. Student at the University of Pittsburgh, Pittsburgh, PA, USA. His research interests include fault diagnosis of traffic equipment, in particular, on bearings and inverters, by means of machine learning.

Wu Xun was born in Xinhua, China, on November 5, 1993. He received the B.E. degree in automation from Central South University (CSU), Changsha, China, in 2011. He is currently working toward the Ph.D. degree in traffic equipment and information engineering at the Institute of Rail Transport and Electric Traction Technology, CSU.

His research interests include rectifier and inverter fault diagnostics, and life-prediction of capacitors.